

43

BEITRÄGE ZUR RADARGRAMMETRIE UND DIGITALEN BILDVERARBEITUNG

CONTRIBUTIONS TO
RADARGRAMMETRY AND
DIGITAL IMAGE PROCESSING

Mitteilungen der Geodätischen Institute der
Technischen Universität in Graz

Folge 33
Graz , 1980

PHOTOGRAMMETRIC DIFFERENTIAL RECTIFICATION
OF RADAR IMAGES ¹⁾

F. Leberl and H. Fuchs
Technical University of Graz, Austria

ABSTRACT

Side-looking radar (SLR) images are available of large areas of the Earth's surface, largely in the form of uncontrolled mosaics of the raw images, compiled to help in small scale reconnaissance surveys.

Orthophotographic radar presentations have traditionally not been available. Some recent efforts to generate rectified radar images were based on digital image processing. The present paper reports on the production of radar orthophotos using a general purpose photogrammetric differential rectifier (Wild Avioplan OR-1). Orthophotos are produced of an area in the USA that was imaged by X-band radar. Data of the inertial navigation and of the digital terrain relief can be an input to the rectification procedure.

The paper emphasizes theoretical considerations and discusses the mathematical model employed; an example of a radar orthophoto is produced and the accuracies are evaluated.

ZUSAMMENFASSUNG

(Photogrammetrische Differentialentzerrung von Radarbildern)

Seitwärtsradarbilder bestehen heute von großen Teilen der Erdoberfläche, vornehmlich in der Form von unkontrollierten Bildmosaiken, die für kleinmaßstäbige Erkundungskartierungen erstellt werden.

Orthophotographische Radardarstellungen wurden bisher kaum erzeugt. Neue Bemühungen auf diesem Gebiet beruhen auf digitaler Bildverarbeitung. Die vorliegende Arbeit berichtet über die Herstellung von Radarorthophotos mittels eines photogrammetrischen Differentialentzerrungsgerätes (Wild Avioplan OR-1). Von einem Gebiet der USA, von dem X-Band Radarbilder vorliegen, wurden Orthophotos hergestellt. Die Daten der Inertialnavigation und eines digitalen Höhenmodelles können zur Differentialentzerrung herangezogen werden.

Der Beitrag behandelt das mathematische Modell, ein Beispiel eines Radarorthophotos wird hergestellt und die Genauigkeit beurteilt.

1) Presented paper, Working Group III/1 on Geometrical Aspects of Remote Sensing, Symposium of Comm. III, Intl. Soc. for Photogrammetry, 30 July - 5 August 1978, Moscow, USSR.

RESUME

(Redrèssement différentiel photogrammétrique d'images radar)

Il existe aujourd'hui une large couverture de la terre par des images d'un radar latéral. On les présente sous forme de mosaïque des images non-redressées, pour aider dans de projets de reconnaissance à petite échelle.

Ce papier présente une méthode de produire une orthophotographie radar à l'aide d'un système orthophotographique Wild Avioplan OR-1. On discute les formules, un exemple d'image radar orthophotographique et les précisions que l'on peut obtenir.

1. INTRODUCTION

Modern computer-controlled photogrammetric differential rectifiers provide the flexibility to produce orthophotographic presentations of images irrespective of their original geometry. MASRY and GIBBONS (1973) presented scan-imagery rectified on an OMI-OP/C orthoprojector, KRAUS (1978) and OTEPKA (1978) demonstrated the application of the WILD-Avioplan OR 1 to aircraft scan images. MASRY et al (1976) used the Gestalt Photomapper for a similar task.

As regards side-looking radar (SLR) imagery, differential rectification has been reported by YORITOMO (1972), using an especially designed radar orthoprinter, by BRYAN et al (1977) using digital image processing, and by MASRY et al (1976) on the Gestalt Photomapper. No efforts have come to our attention that would use on optically projecting photogrammetric orthoprojector for radar. Previous work by LEBERL (1971) on this topic was only theoretical.

We have now completed the development of a procedure to produce orthophotographic radar images using the Wild Avioplan OR 1 orthophoto-equipment.⁺⁾ The procedure can employ images in both slant - or ground - range presentations, and takes advantage of ground control points, a digital height model (DHM) as well as recordings of navigation data (sensor position and attitude).

We have demonstrated this procedure with an example of Goodyear GEMS 1000 synthetic aperture radar (SAR) imagery of Arizona, USA, that was made available through the Working Group on "Geometrical Aspects of Remote Sensing" (KONECNY, 1976).

The paper first describes the required inputs to the equipment and then outlines the procedure to generate these input data. We then present an analysis of errors that we may expect in the radar orthophoto as a result of finite slit length and erroneous relief data. In this context some formulas are derived for the SLR-images of a straight line, a cercle and

^{+) The instrument is at the Austrian Bundesamt für Eich- und Vermessungswesen, Vienna. It was operated for this project by the Institut für Photogrammetrie, Technical University, Vienna.}

a sphere. This is presented in an appendix. We conclude the paper with a presentation of an example of a differentially rectified SLR-image.

2. INPUTS TO THE ORTHOPHOTO-EQUIPMENT

The Wild-Avioplan OR 1 requires that the image coordinates be given that correspond to a square grid in the orthophoto. The principle of operation follows from the paper by STEWARDSON (1976). Figure 1 is taken from KRAUS (1976): a regular grid of points ($P_1(i_1, j_1), P_2(i_2, j_2), \dots$) in the orthophoto is aligned in the direction of the scan-motion of the slit. On a magnetic tape the image coordinates x, y of points $P_1, P_2 \dots$ must be listed as an input to the differential rectification. For orientation purposes, also three orientation points (A, B, C, see Fig. 1) must be given on the magnetic tape. Available slit lengths s are: $s = 3, 5, 8, 12$ or 16 mm. Enlargement between original and orthophoto range between $0.66:1$ and $6.66:1$.

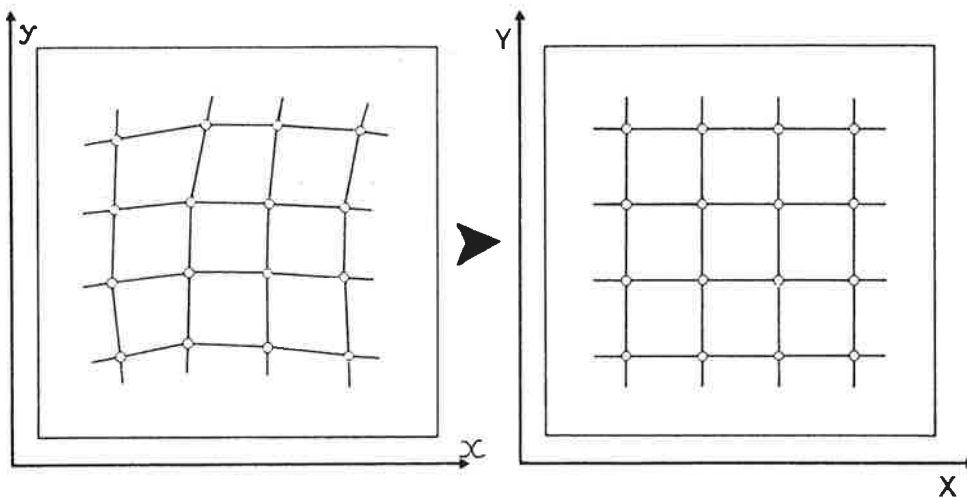


Figure 1: Principle of differential rectification of an arbitrary grid, using the Wild Avioplan OR 1 (from KRAUS, 1976).

3. GENERATION OF INPUTS TO THE ORTHO-PHOTO-EQUIPMENT

We may employ well documented mathematical formulations to obtain the image coordinates that pertain to a given set of object points. The following presentation is based on the work of GRACIE et al (1970), GREVE and COONEY (1974) and LEBERL (1976, 1978).

3.1 Measurements

Measured are

- (a) the object coordinates of control points;
- (b) a Digital Height Model (DHM);
- (c) navigation data, i.e. a list of the sensor's position vector \underline{s} and velocity vector $\underline{\dot{s}}$ (or attitude angles ϕ, ω, κ);
- (d) comparator coordinates of time marks t_1, t_2, \dots , of points on a range reference line (or range marks) and of control points identifiable in the image.

3.2 Transformation of Comparator Measurements into Slant Range r and Time t

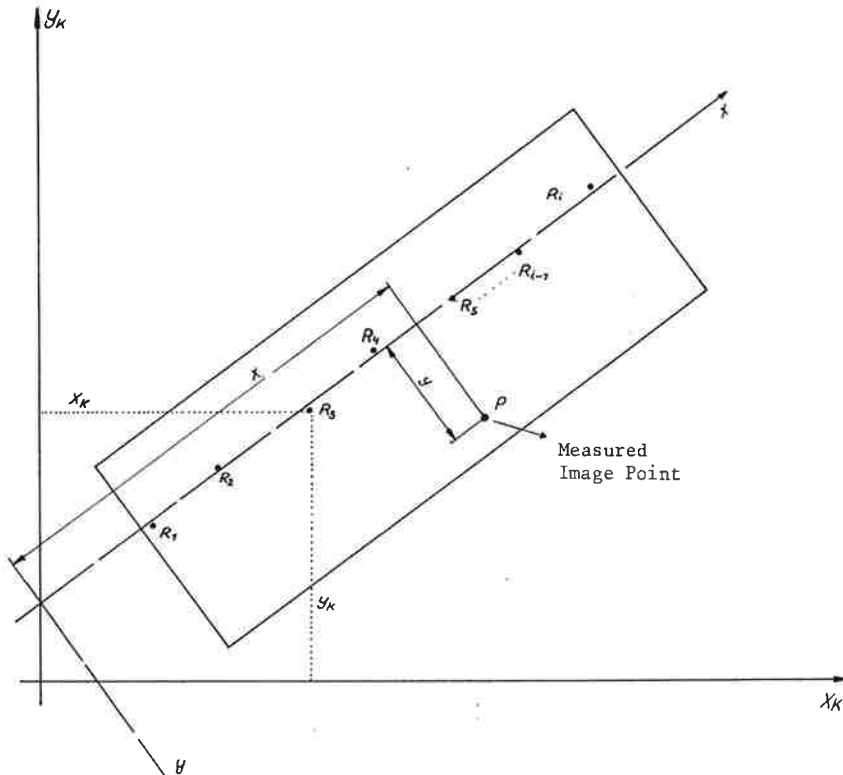


Figure 2: Coordinate systems of the comparator (x_k, y_k) and of the radar image (after GRACIE et al., 1970).

Comparator coordinates x_k, y_k are transformed into image coordinates x, y according to Figure 2 using the following equations:

$$y = (a_1 x_k - y_k + a_0) / (a_1^2 + a_0^2),$$

$$x = (x_k^2 + y_k^2 + a_0^2 - 2 a_0 y_k^2 - y^2)^{1/2}, \quad (1)$$

where a_0, a_1 are the coefficients of the straight line used as a distance reference.

Image coordinates x, y can be converted to time t and slant range r . With the known time t_1, t_2, \dots and $x_1, x_2 \dots$ at time marks $T_1, T_2 \dots$ we obtain:

$$t_p = t_i + \frac{(x - x_i)}{(x_{i+1} - x_i)} \cdot (t_{i+1} - t_i). \quad (2)$$

With the known sweep delay c (slant distance to distance reference line) and image scale factor f we get:

$$r_p = (y + c) f \quad (3)$$

In ground range presentation we need to convert y_g -coordinates with

$$r_p = \{(y_g + e)^2 + H^2/f^2\}^{1/2}, \quad (4)$$

where H is the assumed flight height for the ground range presentation and e is the ground range equivalent to c . If c and f are unknown, than we have in our procedure an option to compute c, f from 2 control points with different y -coordinates. In the event that navigation data, and therefore flight height H , are not available, we compute H also from control points.

3.3 Navigation Data, Control Point Coordinates

Computations take place in a three-dimensional cartesian geocentric or tangential XYZ coordinate system. The navigational data (sensor positions, velocity vector or attitude vector) and control point coordinates must therefore be transformed to geocentric X,Y,Z - coordinates. The navigation data at time t_i ($i = 1, \dots, n$) are assumed to consist of:

Time t_i , longitude λ_i , latitude ϕ_i , barometric or radiometric height H_i .

A new derived set of navigation data is interpolated at equal time intervals $t_0 + i \cdot \Delta t$ ($i = 1, \dots, m$), whereby some filtering of noise is applied and $t_0, \Delta t, m$ are manually chosen entities.

The program system requires that n be at least 2. If navigation data were not actually measured, then they must be approximated for fictitious times t_1, t_2 using control points.

3.4 Digital Height Model (DHM)

A square grid DHM must be input to the procedure. The size of a grid mesh is equal to the slit length. The grid is aligned in the profiling direction of the orthophotoslit. The grid points have the planimetric coordinates $(x_0 + i \cdot \Delta, y_0 + j \cdot \Delta)$, where $i = 1, \dots, k, j = 1, \dots, l$ and Δ is the slit length s in the object coordinate system: $\Delta = s \cdot M$, where M is the scale number of the orthophoto.

The source of the DHM may be topographic maps, photogrammetric stereoplotting, radar stereo plotting etc.

3.5 Computation of Image Coordinates Pertaining to an Object Point P

Given is point P with position vector \underline{g} in the object coordinate system with unit vectors \underline{x} , \underline{y} , \underline{z} (Figure 3). Also given are sensor positions \underline{s}_i and velocity vectors $\dot{\underline{s}}_i$, at times t_i , $i = 1, \dots, n$. The task exists to find the orbit position \underline{s}_g from where point P is imaged. This in turn permits to define time t_g and slant range r_g .

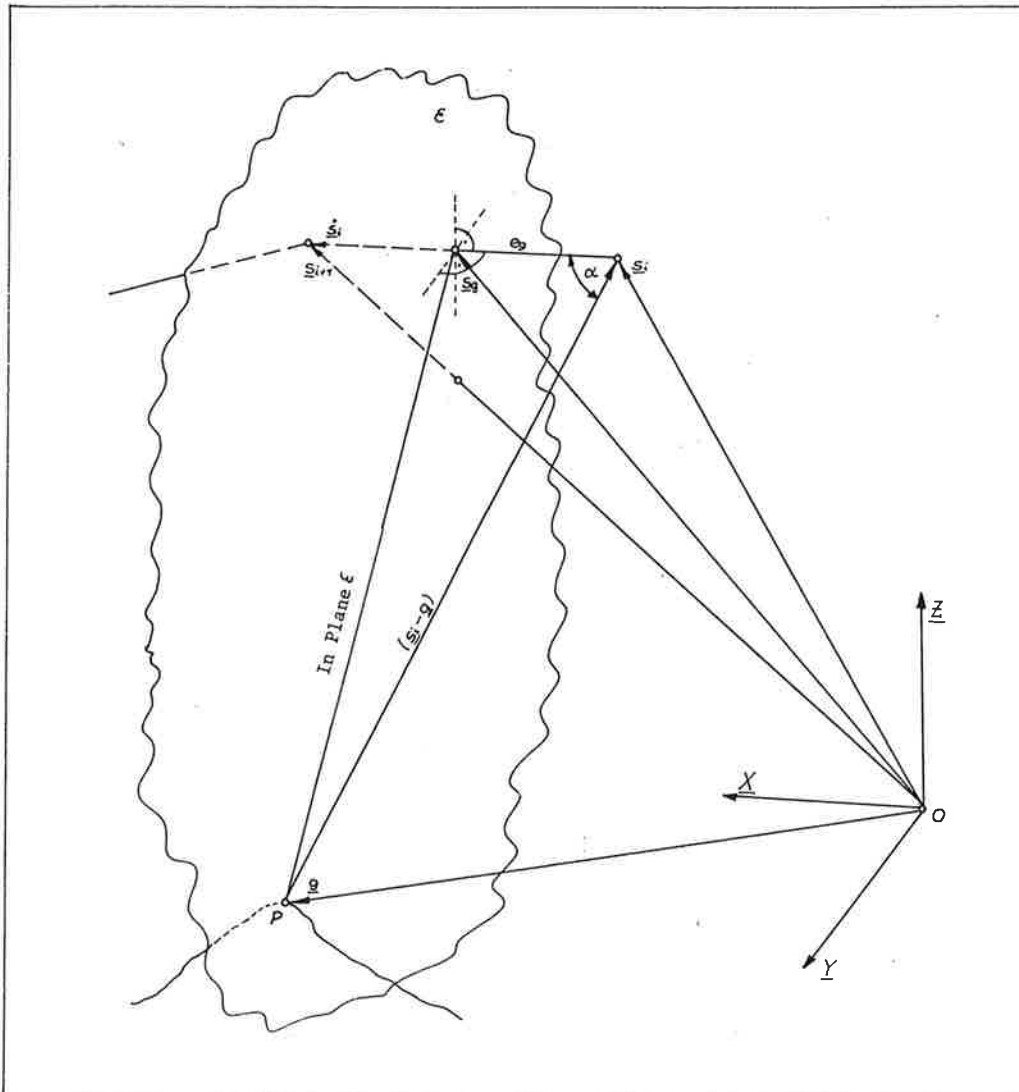


Figure 3: Plane ϵ through point P and normal to vector $\dot{\underline{s}}_i$.

A solution to this task has been used by several authors and was reported in a review by LEBERL (1976):

$$\underline{s}_g = \underline{s}_i + \frac{\dot{\underline{s}}_i}{|\dot{\underline{s}}_i|} e_g, \quad (5)$$

where

$$e_g = \frac{\dot{\underline{s}}_i \cdot (\underline{s}_i - \underline{g})}{|\dot{\underline{s}}_i|}. \quad (6)$$

This leads to:

$$t_g = t_i + \frac{|\underline{s}_g - \underline{s}_i|}{|\dot{\underline{s}}_i|} (t_{i+1} - t_i), \quad (7)$$

$$r_g = |\underline{g} - \underline{s}_g|. \quad (8)$$

Image coordinates x_g, y_g derive from inversion of equs. (2) and (3) or (4).

$$x_g = x_i + \frac{(t_g - t_i)}{t_{i+1} - t_i} (x_{i+1} - x_i), \quad (9)$$

$$y_g = \frac{r_g}{f} - c. \quad (10)$$

3.6 Use of Control Points

Control points are used to improve the x_g, y_g -coordinates of equs. (9) and (10). Their image coordinates x_c, y_c are defined by measurements in the comparator and subsequent transformation acc. to equ. (1). However the procedure of section 3.5 also provides image coordinates of the control points, denoted here by x_g, y_g . We obtain discrepancies

$$\begin{aligned} \Delta x &= x_c - x_g, \\ \Delta y &= y_c - y_g, \end{aligned} \quad (11)$$

which serve to define a correction surface for x_g, y_g coordinates of radar points. As a correction surface we use polynomials of the following type:

$$\Delta x = a_0 + a_1 x + a_2 x^2 + a_3 x^3 \quad (12 a)$$

$$\Delta y = b_0 + b_1 x + b_2 x^2 + b_4 y + b_5 xy + b_6 x^2 y + \dots \quad (12 b)$$

These polynomials were proposed for radar rectification by GRACIE et al (1970). They are linear in y-direction. Not in all cases do we use all elements of these polynomials.

As previously mentioned we may use control points in two additional tasks if the need arises: (a) to compute c, f-parameters in equ. (3), if they are not available, and (b) to define a flight path if no navigation data were measured.

4. AN ANALYSIS OF ERRORS OF DIFFERENTIAL RADAR RECTIFICATION

In the following error analysis we assume that a radar image is given in slant range presentation. With error-free navigation and inner orientation the radar rectification must eliminate image deformations due to:

- (a) slant range presentation ,
- (b) relief displacement.

4.1 Choice of Scan Direction

If scanning is not in range direction but along the image x-axis, then the differential enlargement between image and orthophoto has to be obtained by appropriate zoom-magnification. Scanning in y-direction would achieve differential scale changes by appropriately varying the relative motion of image and orthophotos under the slit.

The differential magnification of the zoom is limited. In the Wild-Avioplan it ranges from 0.4 to 2.5. In a slant range presentation the required scale changes are inversely proportional to the sine of Ω , where Ω is the elevation angle of the line of sight; $1/\sin(\Omega)$ varies from 1 (at far range) to ∞ (at the nadir).

It is obvious then that the overall and the differential magnification both have to be chosen such that for a given set of imaging parameters (Ω_{\min} , Ω_{\max}) one remains within the ranges of the instrument. It is also recommended to choose the scan direction to coincide with the image y-coordinate. In that case the long slit extends in the essentially undistorted x-direction and no errors are caused by the finite slit length if the terrain is flat.

The required scale setting for a given slit position is a function of a number of parameters illustrated in Figure 4:

scan direction , the position of the nadir line as indicated by p, the flight height H, the terrain slope α in the direction of the slit length and the slit position X, Y.

Figure 5 presents graphically the variation of scale values with changing X, α and :

It is obvious that for = 0, there is the smallest variation of the scale number in scan direction (direction of slit motion).

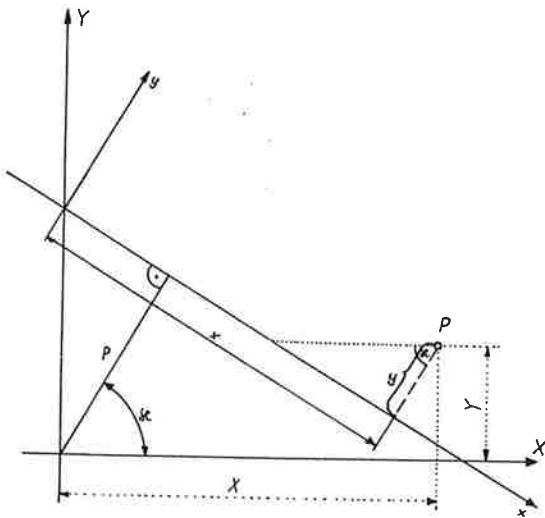


Figure 4: Definitions for the analysis of the effect of scan direction: XY ... system of the orthophoto; x,y ... radar image. Slit moves in X.

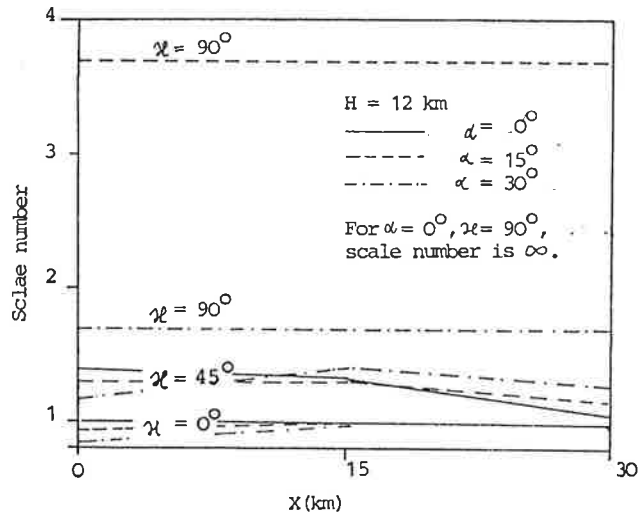


Figure 5: Required enlargements for radar rectification, plotted for different X, χ (compare Figure 4) and terrain slope α (slope X).

4.2 Effect of Finite Slit Length and Terrain Slope

In the previous section we found that if scanning is in y-direction, errors may only be expected for terrain slope $\alpha = 0$.

Figure 6 illustrates that the straight line L' in the orthophoto corresponds to a hyperbola L in the radar image (compare Appendix, equ. A.5), while the straight line element l in the image would correspond to a hyperbola l' in the orthophoto. We therefore get a maximum error ΔY in the orthophoto in the center of the slit.

Figure 7 illustrates the geometric error in the orthophoto due to this effect. We find for slit length $s=8\text{mm}$, slope angle $\alpha = 20^\circ$ that the maximum ΔY -coordinate errors are less than 0.002 mm.

4.3 Effect of Linear Interpolation between Grid Points

We assume again scanning in y-direction. We use a square grid of image points to control the orthophotoproduction. Positions of the scanning slit between grid points are linearly interpolated. As a result line element l in Figure 8 is projected from the image onto the slit L when actually line element L ought to be projected.

Figure 9 presents the magnitude of the resulting errors in the orthophoto. Within the individual grid mesh and the chosen values for terrain slope α , terrain height Z and elevation angle Ω , the error remains less than 0.005 mm.

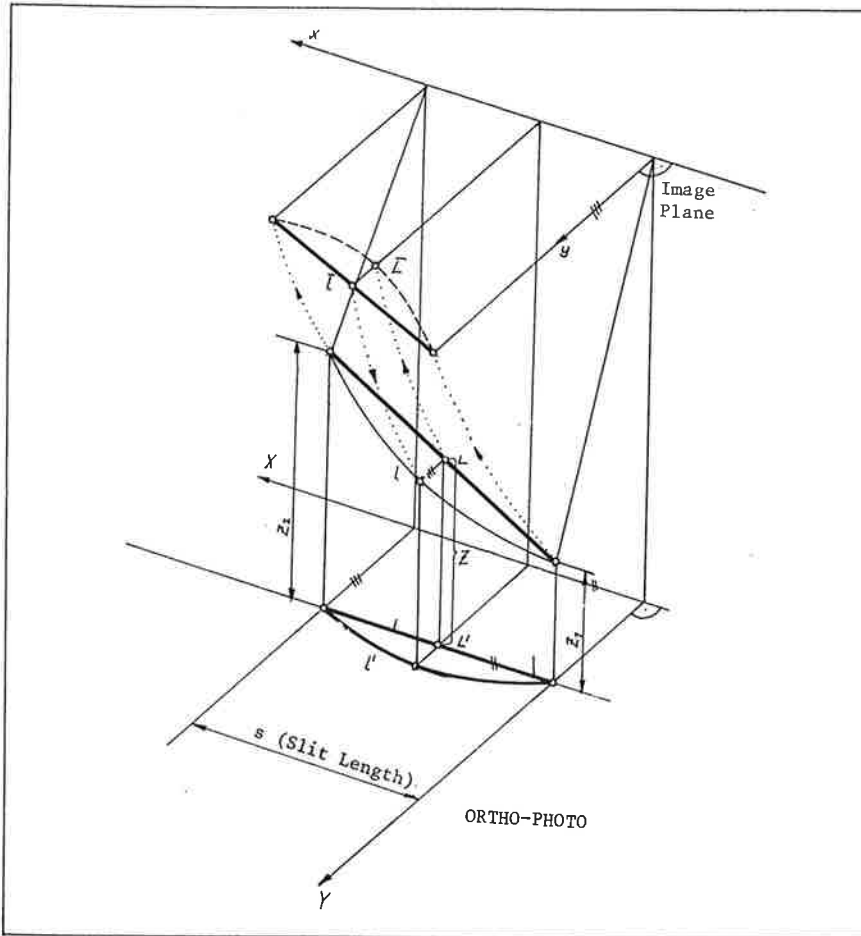


Fig. 6: Combined effect of finite slit length and of terrain slope ($Z_2=Z_1$).

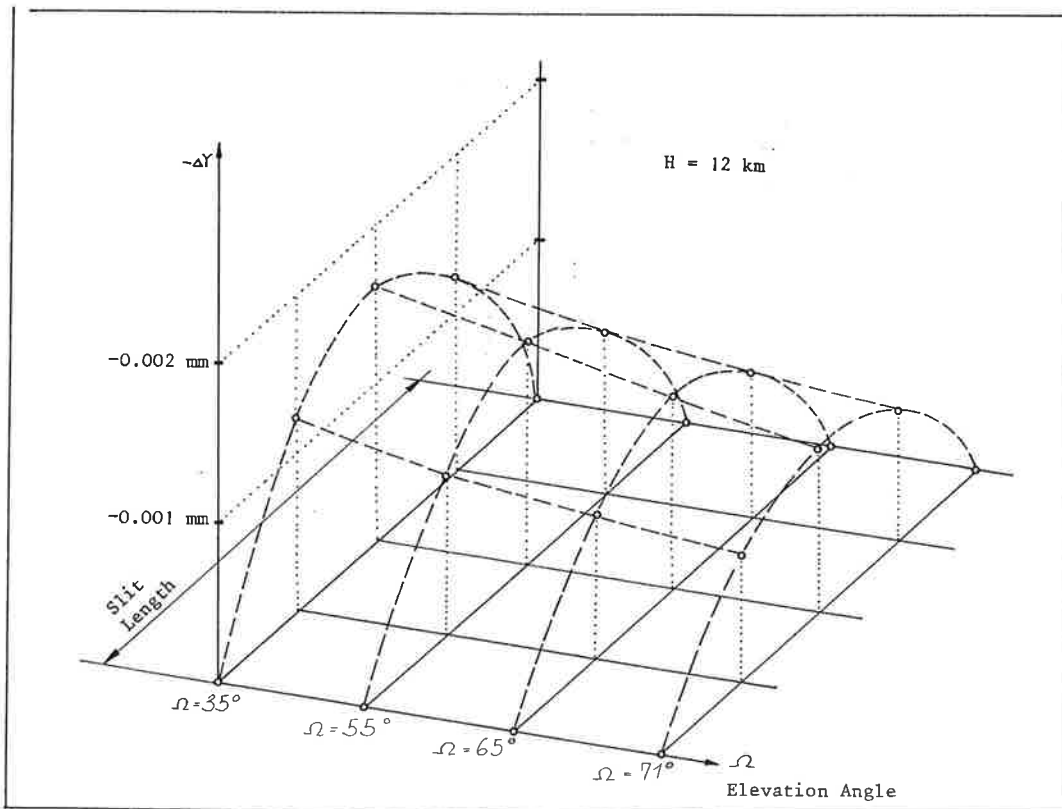


Fig. 7: Maximum error ΔY in the center of the profile in the orthophoto due to the effects shown in Fig. 6. Terrain slope = 20° , slit length = 8 mm.

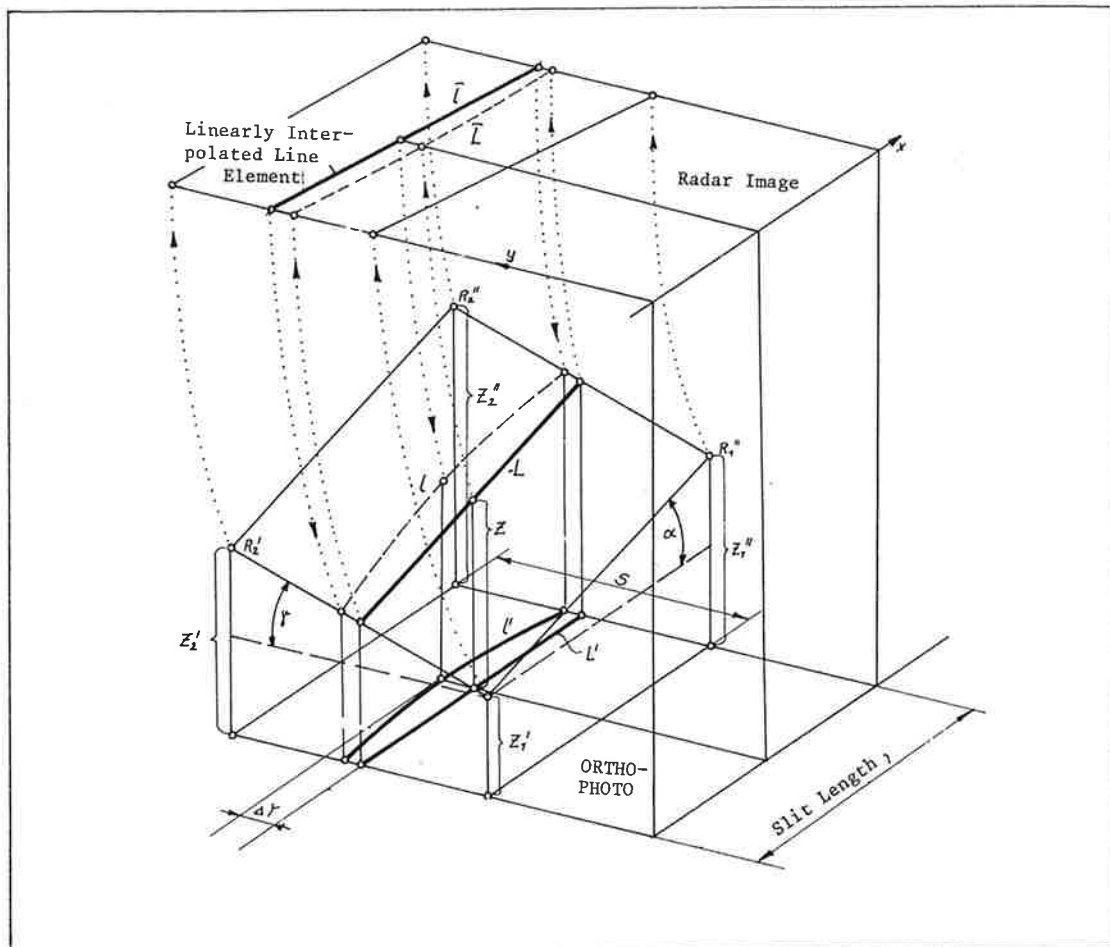


Fig. 8: Effect of linear interpolation between grid points on geometry of radar orthophotos.

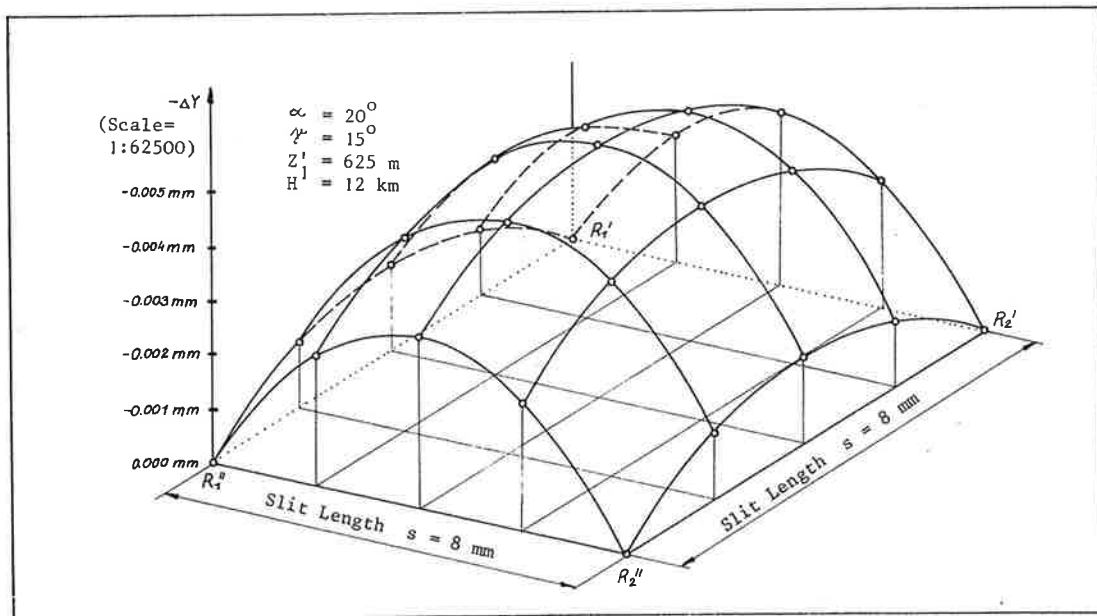


Fig. 9: Errors ΔY due to effects of Fig. 8, presented for one square mesh.

4.4 Effect of Terrain Curvature

Sampling of the terrain relief is along a square grid DHM. The effect of the sampling error can be evaluated by defining the terrain curvature R in addition to its slopes α . As a result one obtains height differences ΔH between actual terrain and the surface interpolated from the DHM. The errors are largest in the center of the square grid mesh. In Figure 10 we show the ΔY -cross track coordinate error in the center of a mesh in the orthophotos as a function of curvature R , slit length s and elevation angle Ω . Also shown is the effect of a random measuring error $H = \pm 1.5$ m.

It is evident from Figure 10 that the sampling error of the terrain heights has an effect far larger than the previously studied errors.

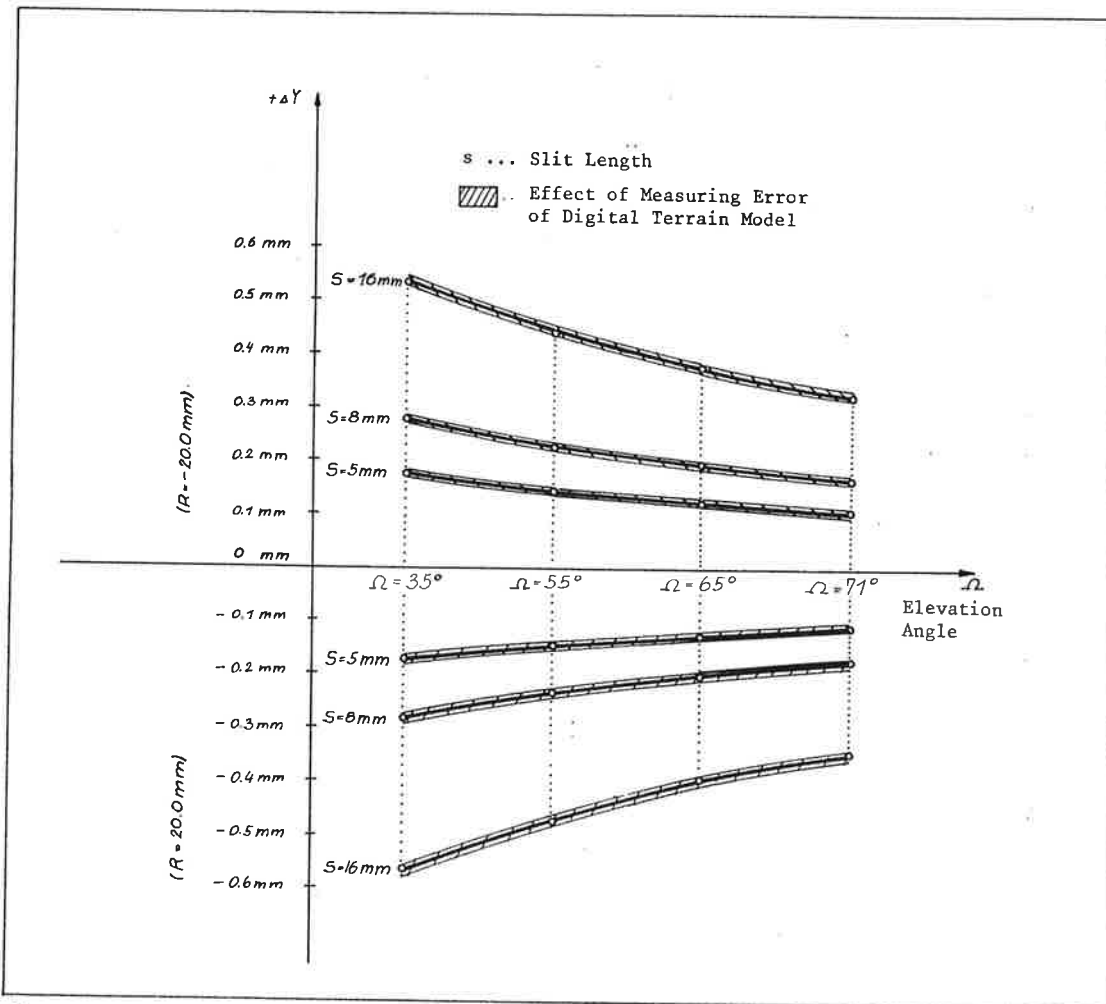


Figure 10: Effect of terrain curvature with radius R on the radar orthophoto. Scale 1: 62 500.

5. EXAMPLE OF RADAR ORTHOPHOTO

5.1 Data, Measurements

The SLR image of Figure 11 shows the Estrella-mountains near Phoenix, Arizona (USA). This image is part of a set that was made available by Goodyear/Aeroservice to the ISP-Working Group on "Geometrical Problems of Remote Sensing". Several studies have been carried out with this material (DERENYI, 1974; DOWIDEIT, 1976). The image was flown from an altitude of 12 km. It presents ground ranges, at a scale 1: 400 000, and is the result of a Synthetic Aperture Radar (SAR) with ground resolution of about 12 meters. Imaging is at elevation angles 36° Ω 75° .

Of the area imaged we also could use a 1:24 000 orthophotomap and 1:62 500 topographic map sheet. However, there were no navigation data recorded, nor were there parameters given for the inner orientation of the imaging system.

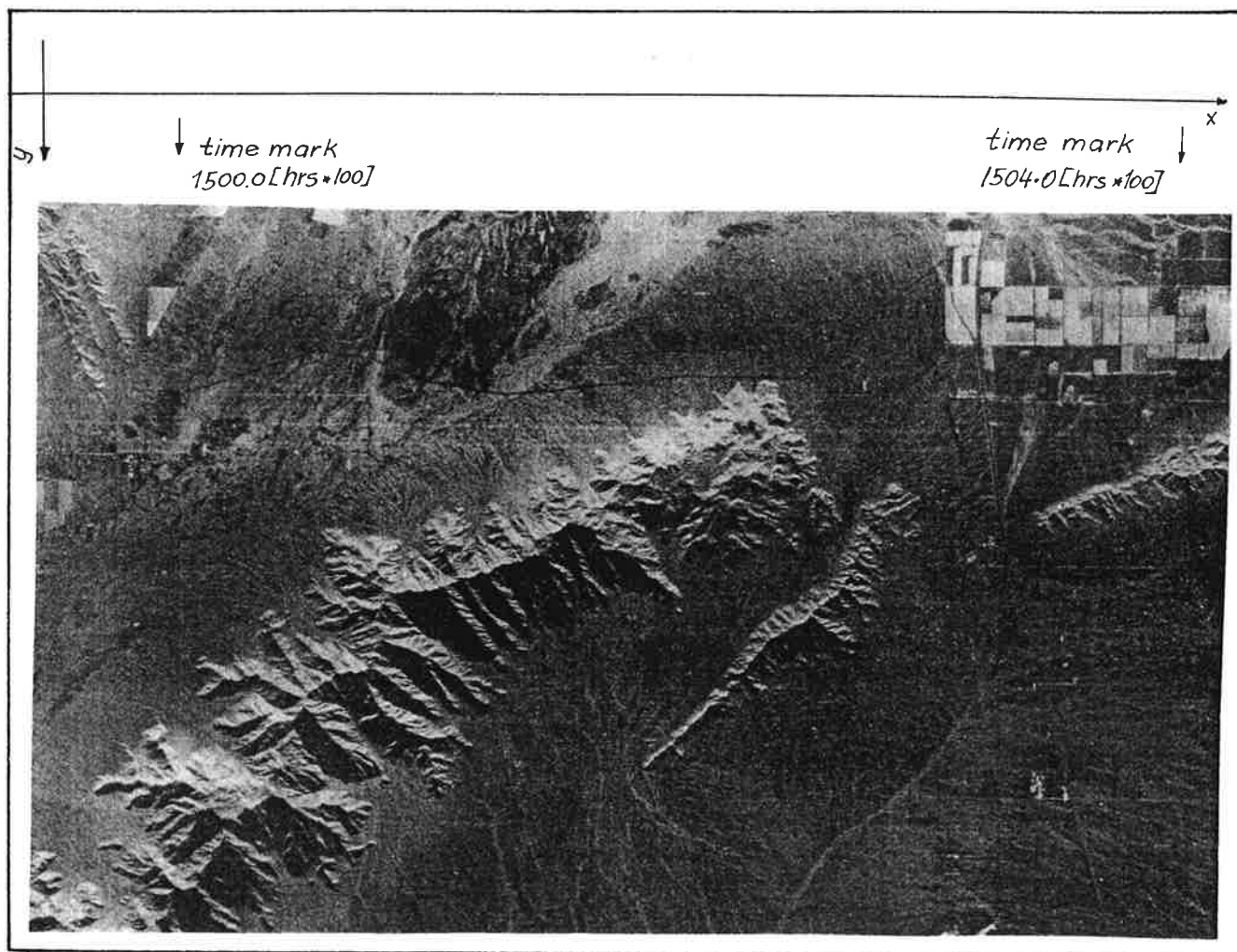


Figure 11: Radar image with coordinate axes x,y and time marks.

The first step was to identify, and measure, a number of 31 control points (Figure 12) in a study area of about 14 km x 16 km, together with a range reference (range marks). The range marks were used to define inner orientation parameters c , f and the flight path with flight height H .

The next step was the acquisition of a DHM with a mesh size equal to the slit length of the orthoprojector, choosing a value $s = 8$ mm, and orthophotoscale 1:62 500. The original image was 2 times enlarged to 1: 200 000, so that in the orthophoto equipment, enlargement is 3.20 : 1. The map 1:62 500 provided the DHM. The accuracy of individual DHM heights as interpolated from the 40 feet (12 m) contours is about 5 m, using the Koppe-standard. In addition to the DHM also the control point coordinates had to be read off the topographic maps.

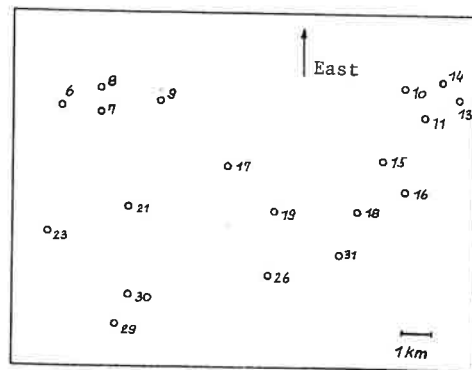


Figure 12: Control and check point distribution in the study area.

Preparation of the input for the orthoprojector followed the procedure of chapter 4.

5.2 Accuracy Analysis

The total of 31 control points was split in two groups, where one group served to rectify the image while the second group was used as check points to evaluate the rectification accuracy. Several different distributions of ground control and of rectification polynomials (see equ. 12) were employed.

Table 1 presents some of the examples that were computed. They confirm single image mapping accuracies obtained by other authors with the same and other radar images (DERENYI, 1975; GOODYEAR, 1974; for a review see LEBERL, 1976). We conclude that the accuracy in cross track (y) is higher than along track, with $y = + 22$ m, $x = + 39$ m. Across-track image errors require bi-linear rectification polynomials, while in along-track direction one needs to employ second order polynomials. Density of control points amounts to 1 to 3 pts per 100 km².

Although these results all are mere confirmations of results that were achieved previously by other authors it should be mentioned here that the study area is not flat. Height differences of up 1000 m exist here, while other studies often relied on images of flat areas.

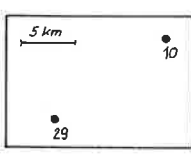
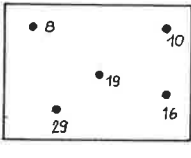
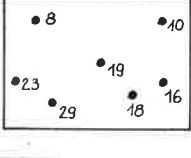
Distribution of Control Points	Polynomials	RMS in X	RMS in Y	Points per 100 km ²
	① $x = a_0 + a_1 x$ $y = b_0 + b_4 y$	$\pm 0.307 \text{ mm}$ $\pm 64.4 \text{ m}$	$\pm 0.349 \text{ mm}$ $\pm 69.8 \text{ m}$	1
	④ $x = a_0 + a_1 x$ $y = b_0 + b_1 x + b_4 y + b_5 xy$	$\pm 0.229 \text{ mm}$ $\pm 45.8 \text{ m}$	$\pm 0.129 \text{ mm}$ $\pm 25.8 \text{ m}$	2
	⑥ $x = a_0 + a_1 x + a_2 x^2$ $y = b_0 + b_1 x + b_4 y + b_5 xy$	$\pm 0.196 \text{ mm}$ $\pm 39.2 \text{ m}$	$\pm 0.110 \text{ mm}$ $\pm 22.0 \text{ m}$	3

Table 1: Residual mapping errors found in check points.

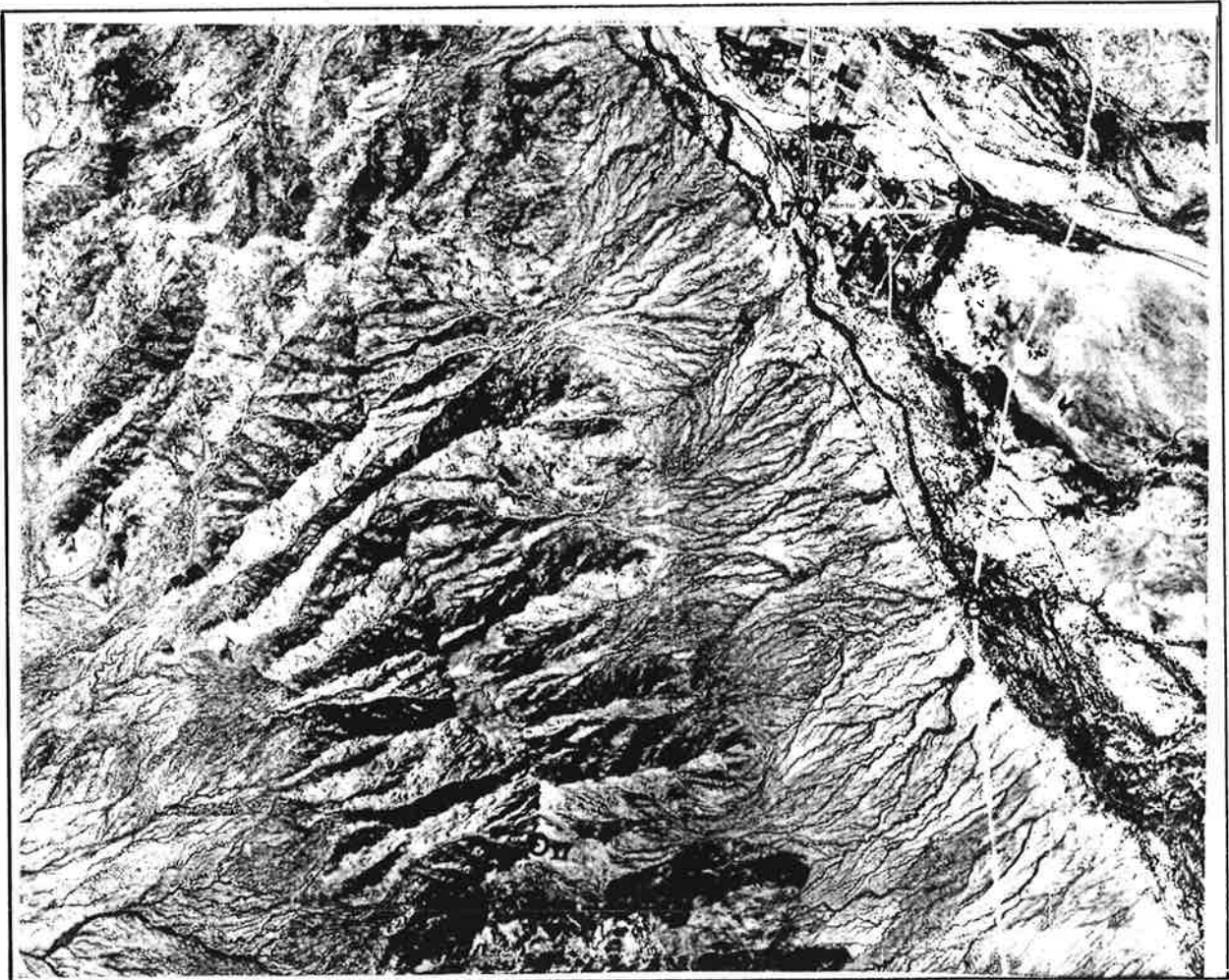


Fig. 13: Section of the orthophotomap of the Estrella Mountain, Montezuma Peak Quadrangle, 7.5 Minute Series, Arizona. Original photography 1: 78 000.

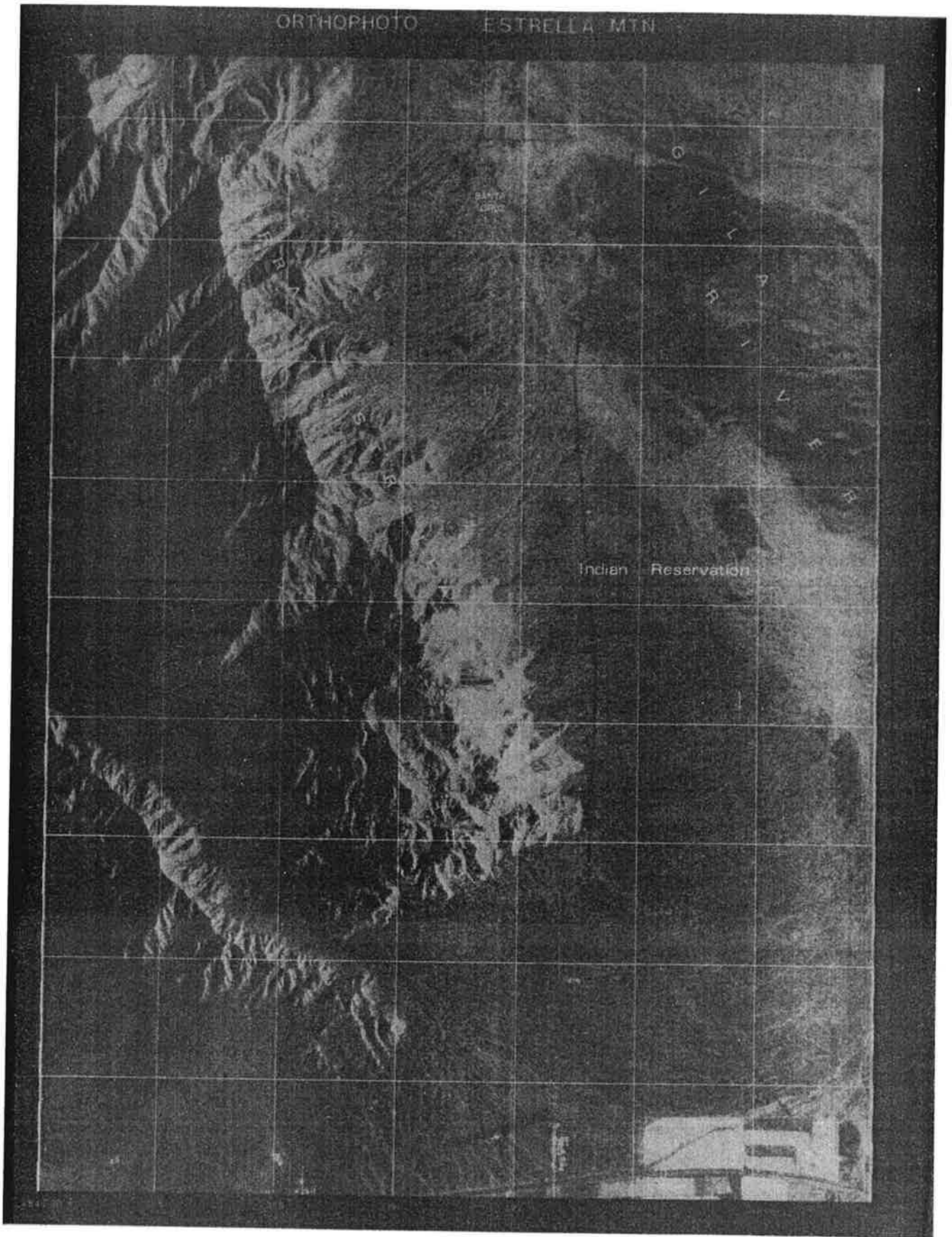


Figure 14: Differentially rectified section of Goodyear GEMS radar image. The UTM-grid has a mesh size of 2 km.

5.3 The Radar - Orthophoto

Figures 13 and 14 present a section of the orthophotographic radar presentation and the orthophotomap of the same area. Differential corrections applied in the rectification amount to about 1 cm at orthophoto scale. Remaining geometric differences with the orthophoto amount to ± 0.1 to ± 0.3 mm (± 6 to ± 19 m) in flats parts, and to ± 0.2 to ± 0.5 mm (± 12 to ± 31 m) in the mountainous area. We can thus conclude that ortho-projection did not introduce any errors, accuracies are the same as those of Table 1.

6. CONCLUSION

Radar images are covering large parts of the Earth's surface. Usually the data are presented in the form of radar - image mosaics for the purpose of subsequent reconnaissance type geoscience interpretation. The image mosaics do not employ (differentially) rectified SLR images. Therefore they are called "semi-controlled", since ground control is used only for the most crude rectification.

Increasingly, however, SLR-data are used in smaller areas for detailed studies, and in conjunction with other remote sensing data (HARRIS and GRAHAM, 1976; NASU and ANDERSON, 1976; SCIENCE, 1977; LEBERL and ELACHI, 1977). This is where a need emerges for differentially rectified remote sensing images. We have demonstrated in this paper the application of a general purpose, computer-controlled analog orthophotoprojector for radar rectification. We could achieve accuracies equal to those of numerical single image mapping.

The procedure used employs the radar image with time- und distance references, navigation data, control points and a digital height model. It has been applied here to one example of imagery. We intend to continue this work and to produce other examples of orthophotographic radar presentations.

ACKNOWLEDGEMENT

The authors wish to thank Prof. Dr. K. KRAUS and his staff at the Institute of Photogrammetry of the Technical University Vienna, Austria, for their help in running the WILD-OR 1 orthoprojector with radar images.

A P P E N D I X

SLR-IMAGE OF A STRAIGHT LINE, CERCLE AND SPHERE

The following considerations were inspired by the work of RINNER (1948, 1966) on the circularly scanning radar (Plan Position Indicator). Here we consider side-looking radar, flown along an undisturbed straight flight path. Coordinate systems x, y (SLR-image) and X, Y, Z (object) are defined, where x is X , and X is in flight direction. We find for this idealized situation:

$$x = X \tag{A.1}$$

$$y = Y/\sin \Omega \tag{A.2}$$

A.1 SLR-Image of a Straight Line

An arbitrary straight line in object space be given by its intersection S ($0, Y_s, 0$) with the XY -coordinate plane and angles α, β (Figure A.1). The sensor moves at flight height Z_o .

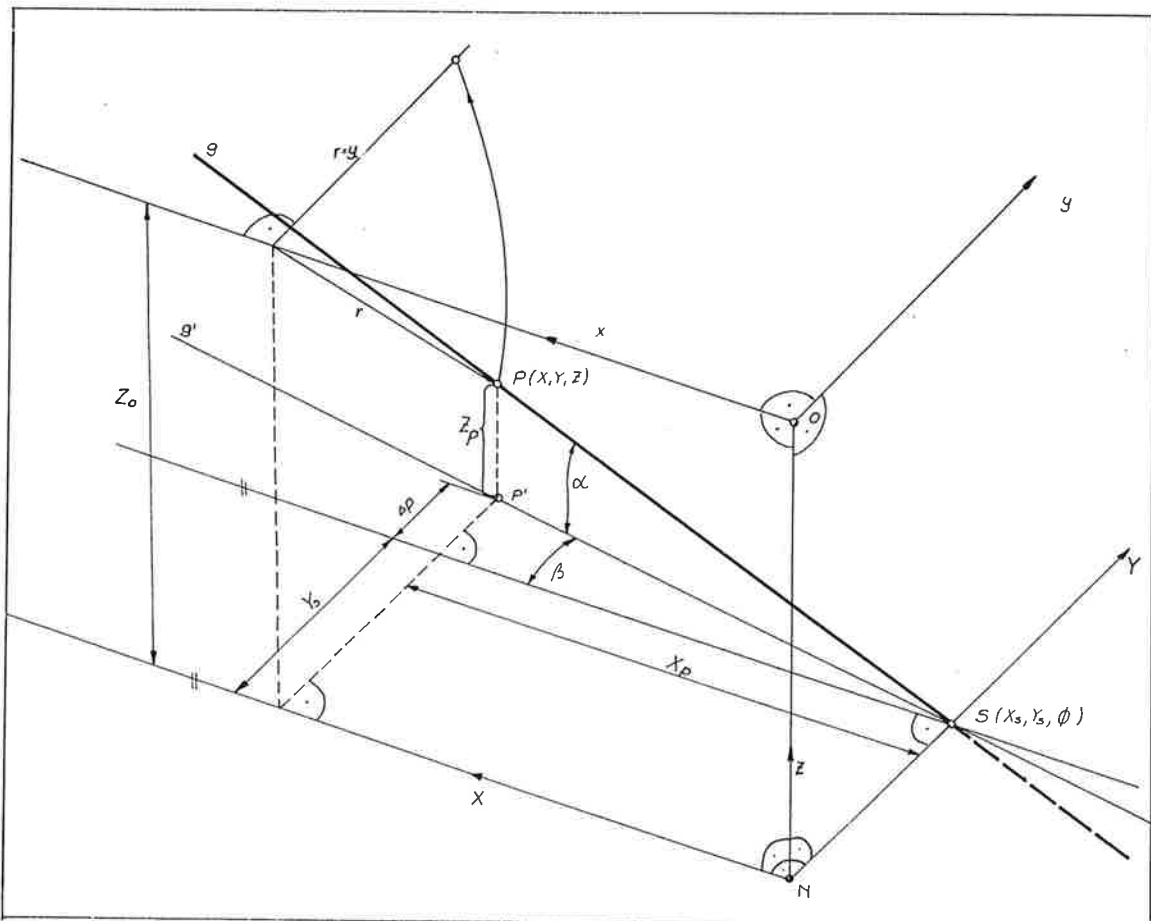


Figure A.1: Straight line g , intersection point S in X, Y, Z system.

We find points P on the straight line:

$$y^2 = (Z_o - Z_p)^2 + (Y_s + X_p \tan \beta)^2 \quad (A.3)$$

and

$$Z_p = X_p \tan \alpha / \cos \beta \quad (A.4)$$

Because of equ. (A.1) we get:

$$y^2 = (Z_o - X \cdot \tan \alpha / \cos \beta)^2 + (Y_s + x \cdot \tan \beta)^2 \quad (A.4)$$

Be rearranging the terms we find for the SLR-image of the straight line defined by S, α , β the following algebraic expression:

$$A x^2 - y^2 + B x + C = 0 \quad (A.5)$$

with:

$$\begin{aligned} A &= \tan^2 \beta + \tan^2 \alpha / \cos^2 \beta \\ B &= -2Z_o \tan \alpha / \cos \beta + 2Y_s \tan \beta \\ C &= Z_o^2 + Y_s^2 \end{aligned}$$

A will always be greater or equal to zero, therefore equ. (A.5) is the equation of a hyperbola. Figure A.2 presents an example for a straight line with $\alpha = 0$, $\beta = 0$. The center M of the hyperbola is on the flight line, where $M = (-B/2A, 0)$. The vertex M has coordinates $N = (-B/2A, (A.C - B^2/4)^{1/2}/A)$.

A.2 SLR-Image of a Cercle

We consider first the SLR-image of a curve in space and then specialize to a cercle. The curve is defined by two equations: the plan view $Y = f(X)$ and the carrying surface $Z = g(X, Y)$ (Figure A.3).

From equ. (A.1) we get:

$$Y = f(x) \quad (A.6)$$

$$Z = g(x, f(x)) = g(x) \quad (A.7)$$

For y we find:

$$y^2 = Y^2 - (Z_o - Z)^2 \quad (A.8)$$

$$f(x)^2 + (Z_o - g(x))^2 - y^2 = 0$$

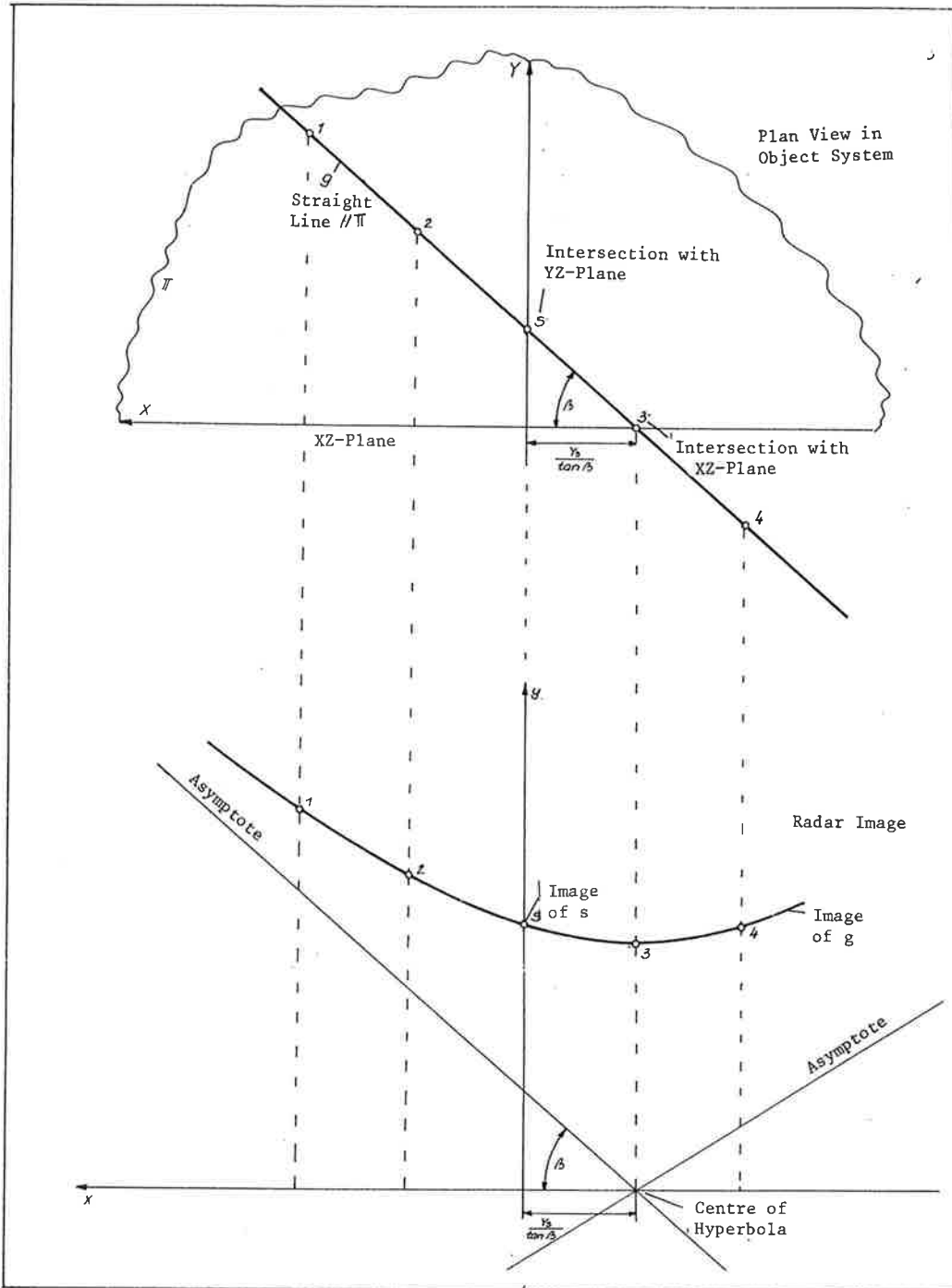


Figure A.2: Radar image of a straight line parallel to XY-plane.

Considering a circle in a plane that is parallel to the XY-plane, eqs. (A.6, A.7) specialize to $(X_M, Y_M \dots$ center of circle):

$$Y = f(x) = R^2 - (X - X_M)^2 \quad 1/2 + Y_M \quad (A.9)$$

$$Z = g(x) = Z_M \text{ (constant)} \quad (A.10)$$

Setting $X_M = 0$, $x = X$ and introducing eqs. (A.9, A.10) in equ.(A.8) we get, after re-arrangements:

$$(x^2 + y^2)^2 + (A^2 - 2B)x^2 - 2B_y^2 + B^2 - A^2 R^2 = 0 \quad (A.11)$$

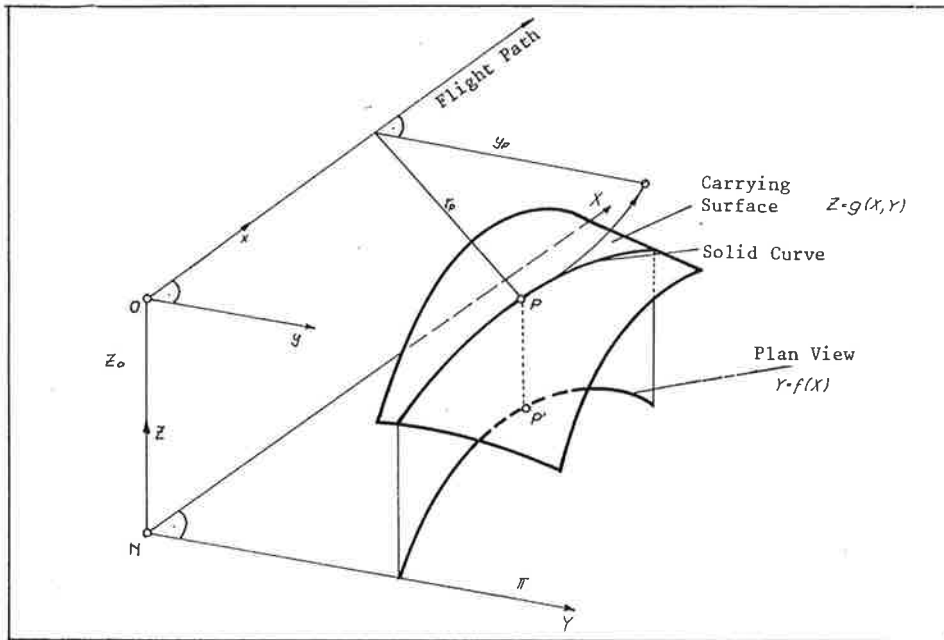


Fig. A.3: Carrying surface $Z=g(X,Y)$, solid curve and plane view $Y=f(X)$

where

$$A = 2Y_M$$

$$B = Y_M^2 + (Z_0 - Z_M)^2 + R^2$$

Equ. (A.11) represents a fourth order curve. For circles, however, with their center in the XZ-plane ($Y_M = 0 \rightarrow A = 0$) we get:

$$y^2 + x^2 = B \tag{A.12}$$

For these circles we also find in the image a circle with radius B .

A.3 SLR-Image of a Sphere

Figure A.4 presents a sphere in object space. Its center M is in the ZY plane, with coordinates $(0, 0, Z_M)$. The contour of the sphere's radar image is defined by points T_i and P_i . We intersect the sphere by a set of planes i normal to the flight line (to the ZY-plane). Each intersection defines a circle. Points T_i are the tangents to the circle and through points I (intersection of i and flight line). Points P_i have the minimum distance between I and the circle.

We find for points T_i :

$$r_M^2 + x_T^2 = y_T^2 + R^2 \tag{A.13}$$

where R is the radius of the sphere, r_M the slant range to the sphere's center M. Because of equ. (A.1) we can set:

$$y_T^2 - x_T^2 = r_M^2 - R^2 \tag{A.14}$$

$$R^2 = X_{Pi}^2 + R_i^2 \tag{A.15}$$

The slant range y_p to points P is with $x_p = X_p$

$$y_p = r_M - (R^2 - x_p^2)^{1/2} \tag{A.16}$$

or

$$x^2 + (y_p - r_M)^2 = R^2 \tag{A.17}$$

which is the image of the cercle of all points P_i .

We see that the sphere's SLR-image consists of a hyperbola and cercle acc. to Figure A.5. Graphical construction of the SLR-image of a sphere is a standard exercise at Remote Sensing Sources at the International Institute for Aerial Surveys and Earth Sciences (ITC), Enschede (compare also LEBERL, 1978 b). An algebraic solution was found by de SOUSA (1973), but never appeared in print.

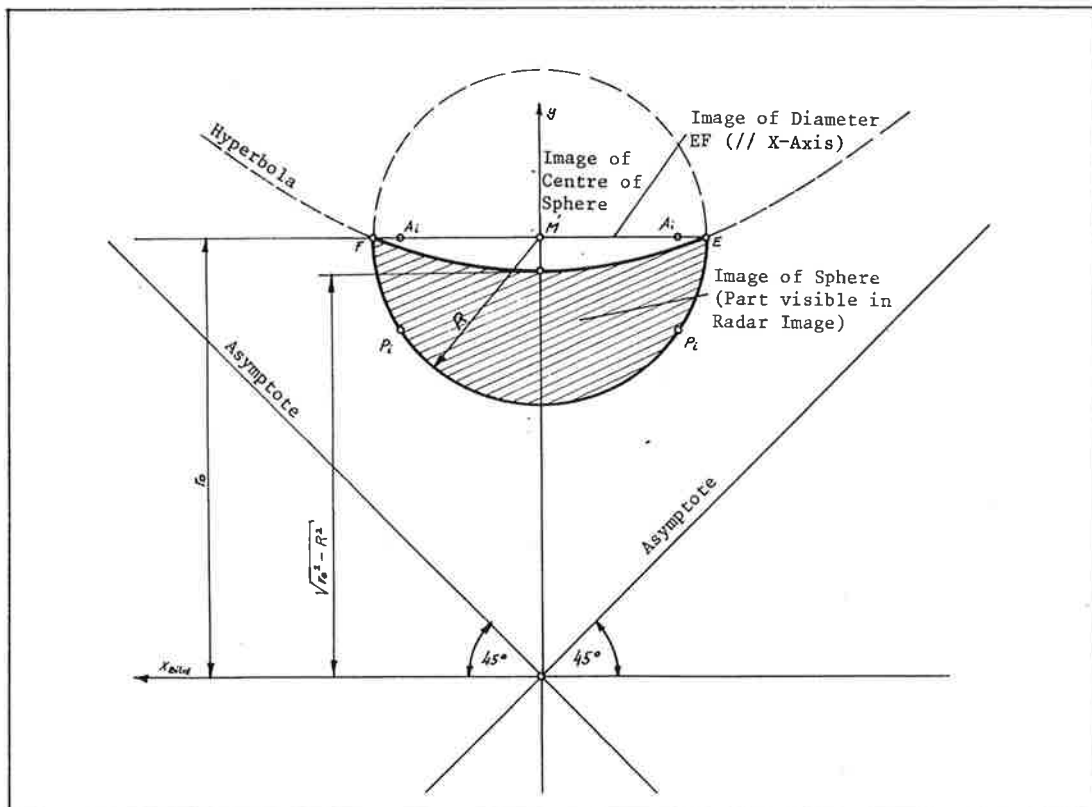


Figure A.5: Image of a sphere in space. Contours consist of hyperbola and cercle.

REFERENCES

- ANDERSON J., M. NASU (1976) A Multi-Series Digital Mapping System for MSS and Photographic Remotely Sensed Data, Presented Paper, Comm. III, 13th Intl. Congress for Photogrammetry, Helsinki, Finland.
- BRYAN M.L., W.D. STROMBERG, T. FARR (1977) Computer Processing of SAR L-Band Imagery, Photogrammetric Engineering and Remote Sensing, Vol. 43, pp. 1283 - 1294.
- DERENYI E.E. (1974) SLAR Geometric Test, Photogrammetric Engineering, Vol. 40, pp. 598 - 604.
- DERENYI E.E. (1975) Topographic Accuracy of Side-Looking Radar Imagery, Bildmessung und Luftbildwesen, Vol. 42.
- GRACIE G. et al. (1970) Stereo Radar Analysis, US Eng. Topographic Labs., Ft. Belvoir, VA, USA, Report Nr. FTR 1339-1.
- GREVE C., W. COONEY (1974) The Digital Rectification of Side-Looking Radar, Proc. Am.Soc. Photogrammetry, Annual Conv., Washington, D.C.
- GOODYEAR (1974) Preliminary Imagery Data Analysis Goodyear Electronic Mapping System GEMS, Report GiB 9342, Code 99696, Goodyear Aerospace Corp., Litchfield, Arizona, USA.
- HARRIS G., L. GRAHAM (1976) Landsat-Radar Synergism, Presented Paper, 13th Intl. Congress for Photogrammetry, Comm. VII, Helsinki, Finland.
- KONECNY G. (1976) Approach and Status of Geometric Restitution of Remote Sensing Imagery, Bildmessung und Luftbildwesen, Vol.43, pp. 2 - 11.
- KRAUS K., (1976) Anwendungsmöglichkeiten eines digital gesteuerten Differentialumbildeggeräts, Geowissenschaftliche Mitteilungen der Technischen Universität Wien, Nr. 8, Vienna, Austria.
- KRAUS K., (1975) Die Entzerrung von Multispektralbildern, Bildmessung und Luftbildwesen, Vol. 43 Nr. 4, also Photogrammetric Engineering and Remote Sensing, Vol. 44, pp. 453 - 457.
- LEBERL F. (1971) Vorschläge zur instrumentellen Entzerrung von Abbildungen mit Seitwärts-Radar (SLAR) und Infrarotabtastsystemen, Bildmessung und Luftbildwesen, Vol.39.
- LEBERL F. (1976) Imaging Radar Applications to Mapping and Charting, Photogrammetria, Vol. 32, pp. 75 - 100.
- LEBERL F., C. ELACHI (1977) Mapping with satellite Side-Looking Radar, Proc., G.D.T.A.-Symp. on Remote Sensing from Aerospace, 21 - 23 Sept., Inst. Géographique National, Paris, France, pp. 451 - 465.
- LEBERL F. (1978 a) Satellitenradargrammetrie, Deutsche Geodätische Kommission, Serie C, Nr. 239, München.
- LEBERL F. (1978 b) "Radargrammetry for Image Interpretation", Revised Edition", ITC-Technical Report Nr. 2, Enschede, Netherlands, 228 p.
- MASRY E., J.G. GIBBONS (1973) "Distortion and Rectification of I.R.", Photogrammetric Engineering, Vol. 32, pp. 845 - 849.
- MASRY S.E., E. DERENYI, B. CRAWLEY (1976) "Photomaps from Non-Conventional Imagery", Photogrammetric Engineering and Remote Sensing, Vol. 42, pp. 497 - 501.

- OTEPKA G. (1976) Practical Experience in the Rectification of MSS Images, Photogrammetric Engineering and Remote Sensing, Vol. 44, pp. 459-467.
- SCIENCE (1977) Remote Sensing, Three Articles in Science Magazine, Vol.196, No. 4289, pp. 511 - 516.
- SOUSA, F. de (1973) The SLR-Image of a Sphere, Unpublished notes prepared for S.A.Hempenius, Intl. Institute for Aerial Survey and Earth Sciences (ITC), Enschede, Netherlands.
- STEWARDSON P.B. (1976) The WILD Avioplan OR 1 Orthophoto System, Presented Paper, Comm. II, 13th Intl. Congress for Photogrammetry, Helsinki, Finland.
- YORITOMO K. (1972) Methods and Instruments for the Restitution of Radar Pictures, Archives, Intl. Soc. Photogrammetry, Invited Paper, Comm.II, 12th Congress, Ottawa, Canada.